# The Immunogenicity of a Proline-Substituted Altered Peptide Ligand toward the Cancer-Associated TEIPP Neoepitope Trh4 Is Unrelated to Complex Stability

Ida Hafstrand,*[,†] Elien M. Doorduijn,[‡] Renhua Sun,*[,†] Anna Talyzina,*[,†] Marjolein Sluijter,[‡] Sara Pellegrino,[x] Tatyana Sandalova,*[,†] Adil Doganay Duru,[{,‖] Thorbald van Hall,[‡,1] and Adnane Achour*[,†,1]

Human cancers frequently display defects in Ag processing and presentation allowing for immune evasion, and they therefore constitute a significant challenge for T cell–based immunotherapy. We have previously demonstrated that the antigenicity of tumor-associated Ags can be significantly enhanced through unconventional residue modifications as a novel tool for MHC class I (MHC-I)–based immunotherapy approaches. We have also previously identified a novel category of cancer neo-epitopes, that is,T cell epitopes associated with impaired peptide processing (TEIPP), that are selectively presented by MHC-I on cells lacking the peptide transporterTAP.In this study, we demonstrate that substitutionof the nonanchoring position3intoa proline residue ofthefirst identified TEIPP peptide,the murineTrh4, resultsin significantly enhanced recognitionby antitumorCTLs towardthe wild-type epitope. Although higher immunogenicity has in most cases been associated with increased MHC/peptide complex stability, our results demonstrate that the overall stability of H-2D$^b$ in complex with the highly immunogenic altered peptide ligandTrh4-p3Pis significantlyreduced compared with wild-typeH-2D$^b$/Trh4.ComparisonofthecrystalstructuresoftheH-2D$^b$/Trh4-p3P and H-2D$^b$/Trh4 complexes revealed that the conformation of the nonconventional methionine anchor residue p5M is altered, deleting its capacity to form adequate sulfur–π interactions with H-2D$^b$ residues, thus reducing the overall longevity of the complex. Collectively, our results indicate that vaccination with Thr4-p3P significantly enhances T cell recognition of targets presenting the wild-type TEIPP epitope and that higher immunogenicity is not necessarily directly related to MHC/peptide complex stability, opening for the possibility to design novel peptide vaccines with reduced MHC/peptide complex stability.

Major histocompatibility complex class I downregu-Ag presentation machinery, including TAP-, tapasin-, and lation represents a significant challenge for suc-proteasome-deficient cancer cells (4–10). Our studies also cessful T cell–based cancer immunotherapy. Indeed, revealed the existence of a broad unique TEIPP-specific T cell immunotherapy studies in melanoma patients have previously repertoire that is highly specific to only Ag presentation mademonstrated that progression of cancer lesions is linked to chinery–deficient cancer cells (5, 8, 10). These TEIPP-specific reduced MHC class I (MHC-I)/peptide cell surface expression, T cells are selected in the thymus, egress with a naive phenowhereas cancer lesions with normal expression regressed in the type, and can be efficiently exploited for immunotherapy same patient (1–3). We have previously demonstrated the ex-against immune-escaped, TAP-deficient tumor cells expressing istence of a new class of hidden MHC-I–presented self-peptides, low levels of MHC-I/peptide complexes (5). However, priming termed T cell epitope associated with impaired peptide pro-of these TEIPP-specific T cells is required through exposition to cessing (TEIPP), that only appear in tumor cells with defective APCs with normal MHC-I expression (11).

We have also recently determined the crystal structure of H-2D$^b$ in complex with the first prototypic TEIPP peptide Trh4 (12). The structure revealed that the peptide takes a noncanonical peptidebinding pattern forming extensive sulfur–π interactions that contribute to the overall complex stability. Indeed, in contrast to all previously reported crystal structures of H-2D$^b$ epitopes, the TEIPP peptide Trh4 (MCLRMTAVM), derived from the commonly expressed cellular protein Trh4 (10, 13), does not contain an asparagine at position 5 and comprises an unusually large number of sulfur-containing residues at positions 1, 2, 5, and 9. The crystal structure of H-2D$^b$/Trh4 combined with site-directed mutagenesis analysis on peptide binding capacity revealed that Trh4 makes primary use of peptide residues p2C, p5M, and p9M for binding, interacting with specific aromatic residues in H-2D$^b$ (12). Indeed, the removal of sulfur atoms through the conservative substitutions of p2C or p5M to α-aminobutyric acid and norleucine, respectively, severely reduced the overall stability of the H-2D$^b$ complexes, indicating the importance of SH–π and van der Waals interactions for the stability of the MHC/peptide complex.

An additional important result from this previous study was that the methionine at peptide position 5 (p5M) in Trh4 significantly alters the conformation of the H-2D$^b$ residues Y156 and H155, both important for T cell recognition, resulting in the formation of a unique MHC/peptide conformer that is essential for recognition by TEIPP-specific T cells (12, 14). Indeed, substitution of the main anchor position p5M in Trh4 to a conventional asparagine, as found in most H-2D$^b$–binding peptides, significantly reduced the overall stability of the MHC/peptide complex and abolished recognition by the H-2D$^b$/Trh4–specific T cell LnB5, indicating the importance of the subtle interplay between p5M and H155 for adequate T cell recognition (12).

In vaccination studies with the TEIPP Ag Trh4 we established that cognate TCR-transgenic T cells poorly respond to the wild-type Trh4 peptide, even though it forms a stable complex with H-2D$^b$ (12). Others and we previously demonstrated that alteration of cancer-associated epitopes at the nonanchoring peptide position 3 to a proline residue in H-2D$^b$–binding epitopes strongly increases the MHC/peptide complex stability and immunogenicity (15–17). The introduced proline residue forms CH–p and van der Waals interactions with the H-2D$^b$ residue Y159 (Supplemental Fig. 1), highly conserved among most known MHC-I alleles. For example, the p3P modification significantly increased the affinity of the H-2D$^b$/gp100$_{25–33}$-specific TCR pMel. Peptide vaccination using the mimotope gp100$_{25–33}$-p3P induced high frequencies of melanoma-specific CTLs in the endogenous CD8$^+$ repertoire and resulted in dramatically enhanced in vivo responses toward melanoma tumors (15). Surprisingly, the enhanced TCR binding was independent from the observed increased stability of the optimized H-2D$^b$/gp100$_{25–33}$ complex and from the interactions formed between p3P and Y159, as demonstrated by progressive mutation of Y159 to phenylalanine, leucine, and alanine, indicating a direct effect of the p3P modification on TCR recognition, most probably through proline-induced rigidification of the presented peptide (18).

In this study, we intended to expand our previous results based on the p3P modification obtained on conventional tumor-associated Ags onto the TEIPP peptide Trh4. We have investigated the characteristics of the p3P modification on the Trh4 epitope and the in vitro and in vivo CTL responses using the TCR-transgenic LnB5 mouse model. Our results demonstrate that vaccination with Trh4p3P induced extremely robust Trh4-specific CTL responses with high frequencies and effector functions, including IFN-g release, downregulation of CD62L, and in vivo killing capacity. Interestingly, and in contrast to the previously studied tumor-associated Ags, although much more immunogenic, the H-2D$^b$/Trh4-p3P complex was clearly less stable on the cell surface as well as in solution compared with the wild-type H-2D$^b$/Thr4 complex. Thus, our results stand in contrast to the present notion that higher immunogenicity is directly linked to higher MHC/peptide complex stability (19), and they indicate that rigidification of the altered peptide ligand combined with absolute molecular mimicry compared with the wild-type neoantigen are key for enhanced TCR recognition. Collectively, our results extend our earlier findings on p3P-exchanged peptide epitopes to TEIPP-directed CTL responses for recognition of cancer cells with low MHC/peptide expression levels. They also demonstrate that this alternative approach may be used within the frame of vaccination strategies to counteract viruses and cancers.

## Materials and Methods

### Cell lines and mice

The tumor cell lines RMA and RMA-S (TAP-2 deficient) have been previously described (6, 10). The CD8$^+$ T cell clone LnB5, specific for H-2D$^b$/Trh4, was generated and cultured as described previously (5, 6). All cells were cultured in complete IMDM medium containing 8% heat-inactivated FCS, 100 U/ml penicillin, 100 mg/ml streptomycin and 2 mM L-glutamine (Invitrogen) at 37˚C in humidified air with 5% $CO_2$. C57BL/6 mice were purchased from Charles River Laboratories. The generation of LnB5-transgenic (tg) mice has been recently described in detail (5). All experiments with mice were approved by the local Inspection for Animal Welfare under the institutional permit from the Dutch government with number AVD116002015271.

### T cell recognition assays

The LnB5 T cell clone (3 3 10$^3$) was mixed overnight in 100 mlofculture medium in the presence of Trh4 peptide variants and splenocytes (50 3 10$^3$). The following day, levels of IFN-g in the supernatants were assessed by sandwich ELISA, as described before (6, 12). The presented data represent mean values obtained from triplicate test wells, and error bars represent the SD of these values.

### Adoptive T cell transfer and peptide vaccination

Single-cell suspensions of LnB5-tg T cells were made by mechanical disruption of spleen and lymph nodes from LnB5-tg C57BL/6 mice (5). Cells were passed through nylon wool for enrichment of T cells, and 3 3 10$^6$ CD8$^+$ T cells in PBS were injected i.v. in syngeneic recipient C57BL/6 mice. The next day, mice were vaccinated s.c. with 50 mg of the 9-mer wild-type Trh4 (MCLRMTAVM) or the p3P peptide variant (MCPRMTAVM) in 100 mlof PBS. The vaccination site was overlaid directly after vaccination with 60 mg of the adjuvant imiquimod-containing cream Aldara (Meda). Peptide vaccination was repeated at day 8 and recombinant human IL-2 (600,000 IU) was injected i.p. at days 8 and 9. T cell activation was measured in blood taken from the tail vein of the mice. To assess IFN-g production by LnB5-tg cells, blood of recipient mice was cultured overnight in the presence of 1 mg/ml wild-type Trh4 peptide. The next day, intracellular cytokine staining was performed as described before (5). Abs used were specific for CD8 (clone 53-6.7), CD45.1 (A20), CD62L (MEL-14) and IFN-g (XMG1.2) (eBioscience). Data were acquired on an LSRFortessa or FACSCalibur (BD Biosciences, San Diego, CA). Analysis was performed with FlowJo software (Tree Star).

The in vivo cytotoxicity assays were performed as previously described (5). In short, C57BL/6 mice were injected with LnB5-tg cells and vaccinated with Trh4 or Trh4-p3P peptide twice. One week after the second vaccination, mice were challenged with CFSE-loaded splenocytes pulsed with either the wild-type Trh4 peptide or the H-2D$^b$–binding control peptide Ad10 (SGPSNTPPEI). Two days after challenge, spleens were harvested and the percentage of specific killing was assessed by flow cytometry.

### Peptide/MHC cell-surface affinity assays

Peptide binding affinities were determined using cell surface expression levels of H-2D$^b$ on peptide-pulsed TAP-deficient RMA-S cells (15). In short, RMA-S cells were pulsed with the HIV-derived H-2D$^d$–binding epitope P18-I10 (RGPGRAFVTI) (20, 21) and the lymphocytic choriomeningitis virus–derived immunodominant H-2D$^b$–binding peptide gp33 (KAVYNFATM) (22), which were used as negative and positive controls, respectively, together with the wild-type Trh4 and the Trh4-p3P altered peptide ligand variant at the indicated concentration at 26˚C overnight (Fig. 1A). Cell surface expression levels of H-2D$^b$/peptide complexes were assessed on RMA-S cells using the monoclonal anti–H-2D$^b$ Ab KH95 (BD Biosciences).

The mean fluorescence intensity (MFI) measured and the peptide binding affinity were calculated using the formula: [(MFI (peptide) 2 MFI (no peptide)]/MFI (no peptide).

### Peptide/MHC cell surface stabilization assays

RMA-S cells were cultured with $10^{-26}$ M of each peptide for 12 h at 26˚C in 5% $CO_2$. Cells were thereafter incubated at 37˚C for 1 h, then washed in cold serum-and peptide-free medium, and resuspended in prewarmed (37˚C) peptide-and serum-free AIM-V medium (Invitrogen) containing 5 mg/ml brefeldin A (Sigma-Aldrich). Cells collected at time points 1, 2, 4, and 6 h were stained with anti–H-2D$^b$ Ab (clone 28-14-8), washed with PBS, and fixed using 1% paraformaldehyde. Cell surface expression of H-2D$^b$ was determined using a BD FACSCalibur (BD Biosciences). The MFI was calculated as indicated above and cell surface H-2D$^b$ expression at time point 1 h for each peptide was defined as 100% MHC/peptide. Data were analyzed using FlowJo software (Tree Star).

### Thermostability measurements using circular dichroism

Circular dichroism measurements were performed in 20 mM $K_2HPO_4$/$KH_2PO_4$ (pH 7.5) using protein concentrations between 0.15 and 0.25 mg/ml (23). Spectra were recorded with a JASCO J-810 spectropolarimeter (JASCO Analytical Instruments, Great Dunmow, U.K.) equipped with a thermoelectric temperature controller in a 2-mm cell. MHC/peptide complex denaturation was measured between 20 and 65˚C at 218 nm with a gradient of 48˚C/h at 0.1˚C increments and an averaging time of 8 s. The melting curves were scaled from 0 to 100%, and the melting temperature ($T_m$) values were extracted using a sigmoidal fit to the individual sample data and averaging the deflection points for each complex. Curves and $T_m$ values are an average of at least two measurements from at least two independent refolding assays per complex. Spectra were analyzed and figures created using GraphPad Prism 7 (GraphPad Software). Statistics were analyzed using a Student t test.

### Preparation and crystallization of the H-2D$^b$/Trh4-p3P MHC-I complex

The altered peptide variant Trh4-p3P in which position 3 was substituted to a proline (MCPRMTAVM) was prepared by microwave-assisted solid-phase synthesis based on F-moc chemistry (24) on a CEM Liberty peptide synthesizer. The peptide was purified by reversed phase HPLC on a Jasco BS997-01 instrument equipped with a Denali C-18 column from Grace Vydac (10 mm, 250 3 22 mm). Refolding and purification of the H-2D$^b$/Trh4-p3P complex was performed according to previously published protocols (20, 22, 25, 26). Crystals for the H-2D$^b$/Trh4-p3P complex were obtained by using the hanging drop vapor diffusion method. The best crystals appeared in 2 M ammonium sulfate, 0.1 M Tris-HCl (pH 8), and 0.5 M NaCl at 4˚C. Two microliters of 3 mg/ml protein solution in 20 mM Tris-HCl (pH 7.5) and 150 mM NaCl was mixed with 1 ml of crystallization reservoir solution, and thereafter equilibrated against 1 ml of well solution at 4˚C.

### Data collection and processing

Data collection for the H-2D$^b$/Trh4-p3P complex was performed under cryogenic conditions (temperature 100 K) at beam line 14.1 (Bessy, Berlin, Germany) to 2.4 A resolution. Crystals were soaked in a cryoprotectant ˚solution containing 20% glycerol before freezing. A total of 600 images were collected, with 0.3˚ oscillation per frame. Data were processed with MOSFLM (27) and AIMLESS (28) from the CCP4 suite. The H-2D$^b$/Trh4p3P complex crystals belong to the I2 space group. Data collection statistics are provided in Supplemental Table I.

### Crystal structure determination and refinement

The crystal structure of the H-2D$^b$/Trh4-p3P complex was determined by molecular replacement using Phaser (29) and the H-2D$^b$/gp33 complex with the peptide omitted (Protein Data Bank code 1S7U) (22, 30) as a search model. The program Phaser found the solution with two molecules in the asymmetric unit. Five percent of the total amount of reflections was set aside for monitoring refinement by $R_{free}$. Refinement of the crystal structure was performed using REFMAC (31) and Phenix (32). A clearly interpretable electron density was observed in the peptide-binding cleft, and the Thr4-p3P peptide could be unambiguously modeled in all MHC complexes within the asymmetric unit. Water molecules were added using COOT (33) and their position was inspected manually. The stereochemistry of the final model of the H-2D$^b$/Trh4-p3P complex was verified with COOT. The final refinement parameters are presented in Supplemental Table I. Figures were created using the program PyMOL (PyMOL Molecular Graphics System, version 1.8; Schro¨dinger).

### Statistical analysis

Statistical analysis was performed using GraphPad Prism 6. A p value , 0.05 was considered statistically significant.

## Results

### The proline-modified Trh4-p3P peptide induces robust CTL responses

We initiated the present study by assessing CTL responses upon peptide vaccination in C57BL/6 mice that received a low number ($3 \times 10^6$) of CD8$^+$ T cells carrying a tg TCR recognizing the H-2D$^b$/Trh4, named LnB5 (5). Peptide vaccination was performed with synthetic short peptides of Trh4 or the adenovirus-derived control Ag Ad10 together with imiquimod adjuvant. A booster vaccination was provided after 1 wk. Although increased frequencies of transgenic LnB5 T cells were detectable after peptide vaccination with Trh4 compared with control peptide (8% versus 2%, respectively, on day 12), the amplitude of the response was weak (Fig. 1A). We then investigated whether the previously described p3P modification (15) of the Trh4 peptide would induce enhanced CTL responses by determining T cell recognition of this peptide in vitro using the LnB5-tg CTLs. The Trh4-p3P peptide induced much stronger CTL activation even at lower peptide concentrations compared with the wild-type Trh4 peptide. Indeed, $IC_{50}$ values were ~ 10-fold increased (Fig. 1B). Next, the effects of the Trh4-p3P peptide were examined in our mouse model with transferred TCR-tg T cells, and our results demonstrate an extremely robust CTL response (Fig. 1C–F). At the peak of the response, 5 d after the booster vaccination, up to 80% of all CD8$^+$ T cells in the blood were tg LnB5 T cells, indicating a remarkable clonal expansion. In contrast, vaccination with the wild-type Trh4 peptide resulted in ,8% LnB5 T cells (Fig. 1C). Furthermore, LnB5-tg T cells activated by the Trh4-p3P peptide displayed robust effector functions, as indicated by significantly higher levels of IFN-g–producing T cells (Fig. 1D), efficient loss of the lymph node homing receptor CD62L (Fig. 1E), and strong in vivo killing of peptide-loaded targets (Fig. 1F). In conclusion, vaccination with Trh4-p3P resulted in significant in vivo proliferation and enhanced effector functions of TEIPP-specific T cells, in contrast to vaccination with the wild-type Trh4 neoepitope. These improvements at the T cell level were even more impressive than those previously observed with the melanomaassociated Ag gp100 (15).

### Proline substitution significantly alters the binding kinetics of Trh4-p3P

We have previously demonstrated that substitution of the third position of the melanoma-associated H-2D$^b$–restricted epitope gp100 to a proline enhanced significant peptide binding and the overall stability of the MHC/peptide complex compared with the wild-type H-2D$^b$/gp100 complex (15, 18). This increased overall stability combined with similar conformations of the modified peptides compared with wild-type epitopes allowed us to enhance significantly cross-reactive CD8$^+$ T cell responses toward conventional cancer targets following vaccination (15). The same effects on increased complex stabilization were also demonstrated for a large ensemble of H-2D$^b$– and H-2K$^b$–restricted cancer-associated peptides (15). In this study, we first compared the affinity of Trh4 and Trh4p3P to H-2D$^b$ using TAP-deficient RMA-S cells as previously described (15, 34, 35) (Fig. 2A). The H-2D$^b$/Trh4 and the proline-substituted variant displayed comparable binding to H-2D$^b$. Because the two curves did not reach a plateau, we cannot

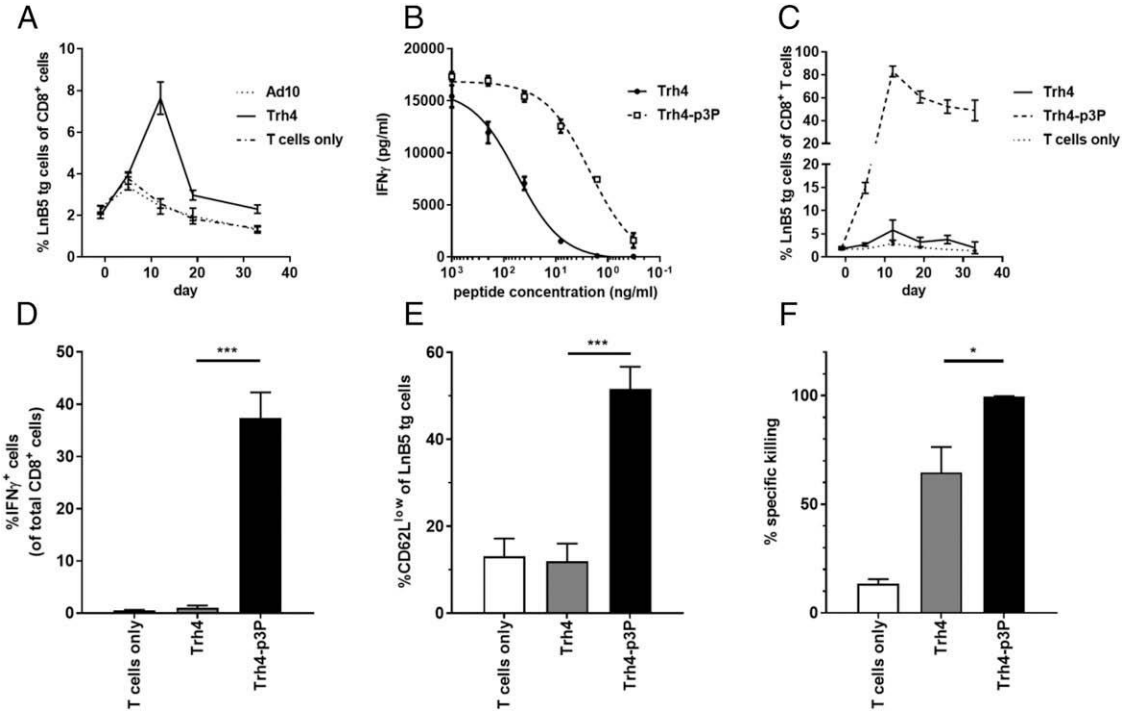


FIGURE 1. Immunization with Trh4-p3P efficiently elicited T cell proliferation and effector functions. (A) Naive wild-type C57BL/6 mice were injected with LnB5-tg cells and vaccinated with wild-type Trh4 or the control peptide Ad10. Blood samples were taken to follow in vivo LnB5 T cell expansion. The presented data are representative of at least two experiments. (B) IFN-g release by the LnB5 T cells in the presence of the wild-type or the Trh4-p3P peptides. T cells were mixed with splenocytes, pulsed with peptide, and IFN-g release was measured by ELISA. Data are shown as mean with SD and are representative of three independent experiments. (C–E) Mice were injected with LnB5-tg T cells and vaccinated with wild-type Trh4 or Trh4-p3P peptides. Blood was analyzed for the presence and activation status of transferred cells after the booster vaccination. Data are pooled from three independent experiments with two to three mice per group. (F) In vivo killing assay in which vaccinated C57BL/6 mice were injected with equal numbers of two differentially CFSE-labeled target cells. $CFSE^{low}$-and $CFSE^{high}$-labeled targets were exogenously pulsed with wild-type Trh4 and a control peptide (Ad10), respectively. Percentage of killing was calculated by the ratio of the two targets in spleens of mice 2 d after challenge. The data represent one experiment including four mice per group and are presented as mean and SEM. *p , 0.05, ***p , 0.001, by Student t test.

calculate accurate $K_D$ values. However, the profiles of the two curves clearly indicate similar affinities.

We also performed both cell surface stability assays (Fig. 2B) and in vitro circular dichroism–based stabilization assays using soluble MHC/peptide complexes (Fig. 2C). Both assays demonstrated that the p3P modification of the Thr4 peptide reduced the overall stability of the H-2D$^b$/Thr4 complex (Fig. 2B, 2C). Most importantly, they demonstrated that Trh4-p3P falls off the cleft of H-2D$^b$ much faster than does wild-type Trh4. Thus, the results presented in Fig. 2 reveal that the binding kinetics for Trh4-p3P are different from wild-type Trh4, where Trh4-p3P both binds faster and falls out faster from H-2D$^b$. Collectively, our results indicate that unlike our previous observations (15), although p3P modification significantly enhanced immunogenicity of the Trh4 epitope (Fig. 1), it reduced the stability of the MHC/peptide complex (Fig. 2).

The crystal structure of H-2D$^b$/Trh4-p3P reveals a conformational modification of the side chain of the main anchor residue p5M that may impact on complex stability

To reconcile the observed very high immunogenicity of Trh4-p3P compared with the wild-type Trh4, with the demonstrated reduced overall stability of H-2D$^b$/Trh4-p3P complexes, we determined the crystal structure of H-2D$^b$/Trh4-p3P (Fig. 3). The structure revealed that this altered peptide ligand is presented by H-2D$^b$ in a nearly identical way as Trh4 (12) (Fig. 4A). In H-2D$^b$/Trh4-p3P, the p3P modification induced a significant conformational change of the side chain of the main anchor residue p5M (Fig. 4B). This modification of the position of the side chain abrogates the SH–p and van der Waals interactions formed between Trh4 and the two aromatic residues W73 and Y156 in the H-2D$^b$/Trh4 complex (Supplemental Fig. 2), and it provides the only reasonable explanation that can be derived from the comparative analysis of the two crystal structures that can explain the lower stability of the H-2D$^b$/Trh4-p3P complex compared with H-2D$^b$/Trh4.

The vast majority of H-2D$^b$–binding epitopes comprises an asparagine residue at position 5 that forms a network of hydrogen bonds with the H-2D$^b$ residues Q97 and Q70 (Fig. 5A) (15, 18, 22, 23, 25, 30, 36). In contrast, the nonconventional methionine p5M in Trh4 cannot form hydrogen bonds. The previously solved crystal structure of the H-2D$^b$/Trh4 complex revealed that in addition to a large ensemble of van der Waals interactions, residue p5M in Trh4 formed sulfur–p interactions with H-2D$^b$ residues W73 and Y156 (11) (Supplemental Fig. 2B). In H-2D$^b$/Trh4-p3P, the modification of the leucine residue at position 3 to a proline affected profoundly the conformation of the side chain of p5M, which rotates and moves closer to the introduced proline residue toward the N-terminal part of the peptide-binding cleft (Fig. 4A, Supplemental Fig. 2C). Consequently, the increased distances between the sulfur tip of p5M and the aromatic rings of residues W73 and Y156 impair the formation of sulfur–p and van der Waals interactions betweenp5M andthese twoH-2D$^b$ residues in H-2D$^b$/Trh4-p3P. Furthermore, the side chain of p5M is localized closer to the polar residue Q97, which is energetically adverse (Supplemental Fig. 2D). Collectively, these structural differences provide a reasonable explanation for the observed lower stability of H-2D$^b$/Trh4-p3P compared with H-2D$^b$/Trh4.

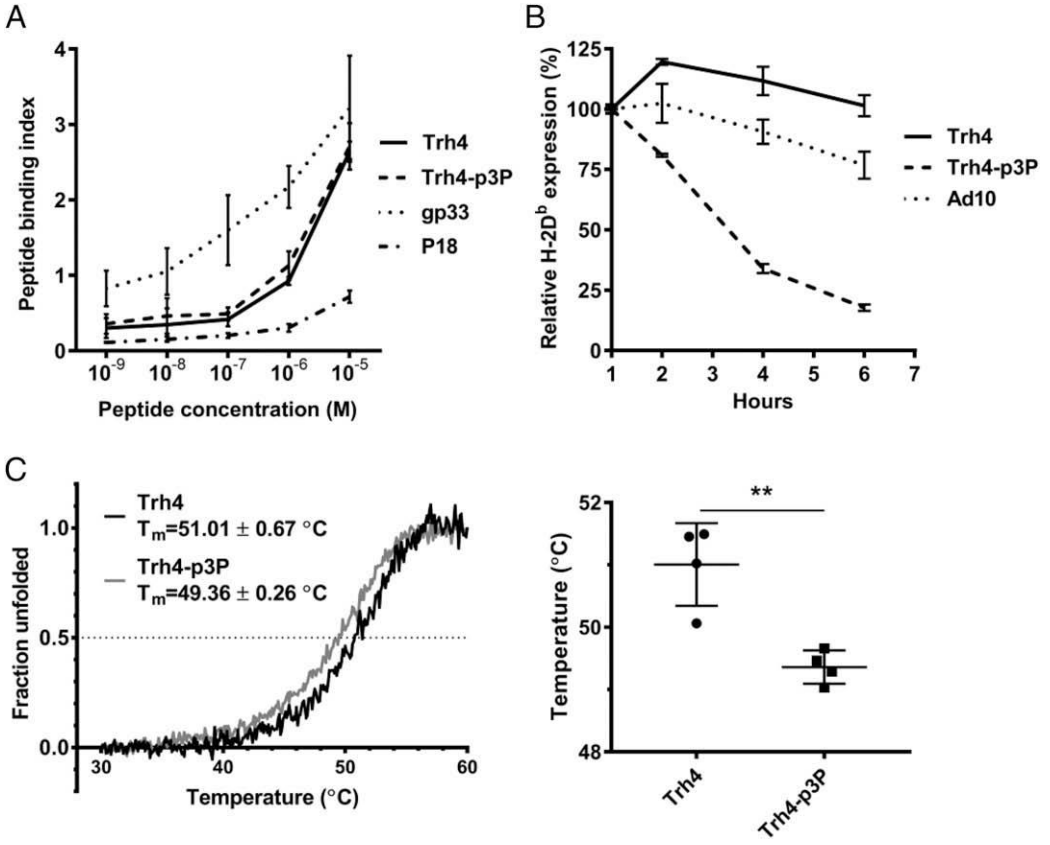


FIGURE 2. Modification of peptide position 3 significantly reduces the overall stability of H-2D$^b$/Trh4-p3P compared with H-2D$^b$/Trh4. (A) The Trh4-p3P and the wild-type Trh4 peptides bind with equivalent efficiency to H-2D$^b$ as measured by MHC H-2D$^b$ cell surface expression on RMA-S cells. The H-2D$^b$–binding lymphocytic choriomeningitis virus–derived peptide gp33 and the H-2D$^d$–binding HIV-derived peptide P18-I10 were used as positive and negative controls, respectively. The presented results correspond to three independent experiments. (B) MHC/peptide stabilization assays using peptide-pulsed RMA-S cells ($10^{26}$ M) reveal that cell-surface expression of H-2D$^b$ in complex with Trh4-p3P is significantly reduced compared with H-2D$^b$/Trh4. The data are represented as mean and SD and correspond to two independent experiments. (C) Left panel, Circular dichroism denaturation curves of soluble H-2D$^b$/Tr4-p3P (gray line) and H-2D$^b$/Trh4 (black line) demonstrate a decrease of 1.65°C in thermostability for Trh4-p3P compared with the wild-type Trh4 peptide. The indicated $T_m$ values correspond to 50% denaturation for each complex. The graphs are normalized averages of four independent measurements for each MHC/peptide complex. Right panel, The $T_m$ values are statistically significant, with a p value of 0.0037 as determined using a Student t test. **p , 0.005.

The surfaces of H-2D$^b$/Trh4 and H-2D$^b$/Trh4-p3P are similar, allowing for TCR cross-reactivity

The conformational shift of the tip of residue p5M in Trh4-p3P also alters the positioning of the H-2D$^b$ residues H155 and Y156, which both move by 0.8 A (Fig. 5C). The conformation of all other °H-2D$^b$ residues remained nearly identical between H-2D$^b$/Trh4 and H-2D$^b$/Trh4-p3P. Whereas the side chain of Y156 moves down toward the bottom of the peptide-binding cleft of H-2D$^b$, the side chain of residue H155 moves up toward the solvent and is more readily available for interactions with TCRs (Supplemental Fig. 2C). However, note that the overall surfaces of H-2D$^b$/Trh4 and H-2D$^b$/Trh4-p3P remain highly similar, allowing for TCR cross-reactivity (Fig. 5). Ultimately, only the determination of the crystal structures of the TCR LnB5 in complex with H-2D$^b$/Trh4 and H-2D$^b$/Trh4-p3P will prove a structural basis underlying both the demonstrated cross-reactivity and the enhanced TCR recognition of the p3P-modified APL.

## Discussion

Upon selection pressure of immune-mediated therapies on cancer lesions, immune-refractory tumor cells frequently escape from CD8$^+$ T cell recognition by abrogating MHC-I Ag presentation. In particular, deficiencies in processing proteins, including the TAP, significantly decrease surface display of MHC-I/peptide complexes (37–39). MHC-I–presented TEIPP epitopes constitute a novel category of immunogenic neoantigens that are presented only on TAP-deficient cells (4, 5, 9, 10, 12). Although derived from endogenous proteins, the ubiquitous TEIPP neoepitopes are nonmutated self-antigens that are not presented on normal cells (11), act as unmasked immunogenic epitopes during tumor immune evasion, and are targeted by a unique category of cytotoxic T lymphocytes (10).

Owing to the weak immunogenicity of the prototype TEIPP Ag H-2D$^b$/Trh4, we investigated approaches to improve its T cell activating capacity. The main working template for modifications that may improve binding to MHC and increase TCR response has to our knowledge most commonly been to complement the interactions between main peptide anchor residues and MHC pockets, sometimes with great success (40, 41). Unfortunately, this approach did not work well for several antigenic peptides, most of the time due to conformational modifications and/or higher flexibility of sections of the modified epitope. In contrast, we focused our attention on the possibility to modify non-anchoring peptide residues. We have previously demonstrated for several tumor-associated epitopes that proline substitution of the nonanchor residue at position 3 substantially increased the overall stability of the MHC/peptide complexes without altering the conformation of the altered peptide ligands compared with the

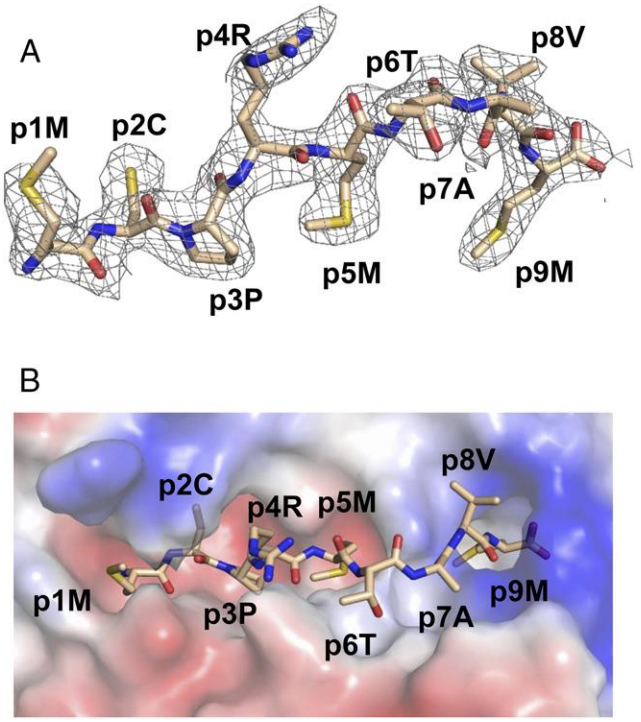


FIGURE 3. The overall structure of H-2D$^b$/Trh4-p3P reveals a non-canonical binding pattern, nearly identical to Trh4. (A) The 2Fo-Fc electron density map of Trh4-p3P bound to H-2D$^b$ contoured at 1.0 s allows for unambiguous positioning of all side chains. The peptide is depicted with the N and C termini to the left and right, respectively. Residues p1M, p4R, p6T, p7A, and p8V protrude toward the TCR. Residues p2C, p3P, p5M, and p9M are buried within the peptide-binding cleft of H-2D$^b$. (B) Top view of the surface of H-2D$^b$ in complex with Trh4-p3P. The negative and positive electrostatic charges are colored in red and blue, respectively. The Thr4-p3P epitope is represented as sticks.

original cancer-associated epitopes (15, 18). Other research groups have applied our peptide modification in a CMV-based vaccine to protect mice efficiently against melanoma (16, 17). Although not always true, it is widely thought that the overall stability and longevity of MHC/peptide complexes is directly linked to their immunogenicity (19, 42, 43). Until now, our own previous studies on conventional overexpressed cancer-and pathogen-associated Ags have hitherto corroborated this view (15, 18, 23). Accordingly, p3P modification of the melanomaassociated H-2D$^b$–binding epitope gp100 resulted in significantly increased stability and immunogenicity. This was also true for a large array of H-2D$^b$– and H-2K$^b$–binding cancer-associated peptides (15). However, to our surprise, the results presented within this study revealed that p3P modification of the TEIPP peptide Trh4 actually decreased significantly the overall stability of H-2D$^b$ in complex with this APL compared with H-2D$^b$/Trh4 and affected the binding kinetics of Trh4-p3P compared with Trh4, with faster $k_{on}$ and $k_{off}$ values. Note that a still limited amount of other studies has also demonstrated that high peptide immunogenicity is not always coupled to higher stability of the MHC/peptide complexes. Instead, it has been proposed that the observed immunogenicity could be modulated by the intrinsic flexibility of specific portions of the presented peptides and/or specific residues on the MHC H chain following "anchor-fixing" modifications (44–47). In our opinion, the results presented in the present study differ from these previous studies, because 1) we do not observe any flexibility in the main chain of the peptide upon comparing the crystal structures of the wild-type Trh4 with the proline-modified variant, and 2) our results demonstrate that the introduction of a proline in the targeted peptide enhances TCR recognition independently from the overall stability of the MHC/peptide complex. In this study, we speculate that rigidification of the MHC/peptide complex due to the substitution of peptide position 3 to a proline facilitates TCR docking and recognition, resulting in stronger CD8 T cell responses. Indeed, irrefragable proofs for the key role of proline residues in increasing the thermostability of proteins and/or protein segments have been previously provided (48, 49). For example, rigidification of the CDRs of Abs or TCRs, sometimes through mutation(s) of the loops residues to prolines, resulted in enhanced affinity to their targets (50, 51). Another nonexcluding possibility is that the p3P modification of the TEIPP peptide Trh4 increases substantially its resistance to proteolysis, which would result in longer survival of the APL following vaccination, and thus possibly enhanced presentation by APCs. Indeed, it has been previously demonstrated that proline motifs in peptide chains and proteins reduce proteolysis significantly. Only a limited number of peptidases are known to be able to hydrolyze proline-adjacent bonds (52).

We have previously demonstrated the importance of SH–p interactions formed between p5M and H-2D$^b$ residues for the stability of the MHC/peptide complex (12). Indeed, modification of p5M to a norleucine reduced drastically the overall stability of the MHC/peptide complex. Furthermore, the crystal structure of H-2D$^b$ in complex with the norleucine-substituted variant of Trh4 revealed that the conformation of the norleucine residue was identical to p5M in the wild-type Trh4. Thus, SH–p interactions are essential for Trh4 binding to H-2D$^b$, and the conformational

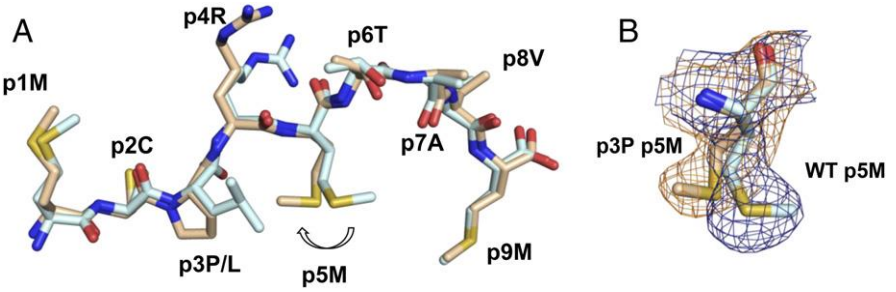


FIGURE 4. The p3P modification impairs the formation of sulfur–p interactions between the nonconventional main anchor p5M and H-2D$^b$ residues. (A) The conformation of the wild-type Trh4 (5E8N, light cyan) and Trh4-p3P (wheat) peptides is nearly identical. The peptides are depicted with their N termini to the left and their C termini to the right, following superimposition of H-2D$^b$ residues 3–173. The side chains of residues at position 1, 4, 6, and 8 of both peptides assume similar conformations. The p3P substitution results in a significant conformational shift of the side chain of peptide residue p5M. (B) Omit maps (contoured at 1.0 s in orange and blue for Trh4-p3P and Trh4, respectively) unambiguously demonstrate a conformational shift of the side chain of p5M in H-2D$^b$/Trh4-p3P compared with H-2D$^b$/Trh4.

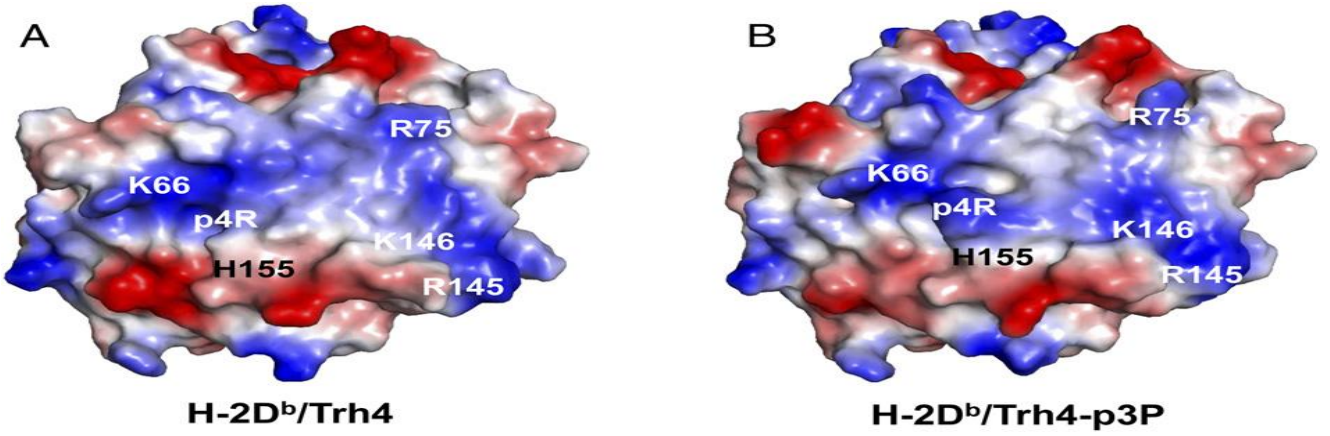


modification revealed by the crystal structure of the H-2D$^b$/Trh4-p3P complex solved in the present study reveals a conformational modification of p5M following the p3P substitution, which abrogates SH–p interactions, explaining the observed reduced stability of the MHC/peptide complex.

In a previous study, we have demonstrated that the interactions formed between p3P in the modified peptide gp100 and the aromatic ring of H-2D$^b$ residue Y159 are essential for the increased stability of the MHC/peptide complex (18). Progressive mutation of residue Y159 to phenylalanine, leucine, and alanine reduced dramatically the overall stability of H-2D$^b$/gp100. However, an important result from the same study demonstrated that the p3P modification allowed for identical affinity of the soluble TCR to H-2D$^b$/gp100-p3P and H-2D$^b$-Y159F/ gp100-p3P. Thus, the rigidification of the peptide following the mutation of position 3 to a proline was enough to keep a similar recognition by the TCR although the Y159F-modified complex displayed lower overall stability (18). In the H-2D$^b$/Trh4-p3P structure, it is evident that this interaction still exists (Supplemental Fig. 2), possibly contributing to the increased immunogenicity of this epitope.

In the present study, our results demonstrate that despite a significant impact of the p3P modification on the kinetic stability of Trh4-p3P compared with Trh4, the rigidification imposed by the proline residue on the peptide enhances considerably functional recognition by the TCR compared with the wild-type epitope. Until further studies are performed, only speculations can be made about the structural reasons underlying the faster kinetics for Trh4-p3P compared with Trh4. One clear possibility for the faster binding rate for Thr4-p3P could be due to rigidification of this APL following the introduction of a proline residue. This could allow for more efficient and thus faster binding. The reasons underlying the faster $k_{off}$ for Trh4-p3P are due to the conformational modification of residue p5M, which is unfavorable as already described above. Still, although displaying a faster binding and a faster fallout to and from H-2D$^b$, this APL elicits significant functional responses by T cells. A future structural comparison of H-2D$^b$/Trh4-p3P before and after binding to the TCR LnB5 should provide a more definite understanding of this phenomenon.

Altogether, this is to our knowledge a novel result that should be taken in consideration upon designing new altered versions of pathogen or cancer-associated epitopes or in the identification of potential MHC-restricted epitopes. Although the results presented within this study are based on only one specific peptide and its recognition by one H-2D$^b$/Trh4–specific TCR LnB5, they clearly indicate that we should not eliminate the functional testing of epitopes with reduced overall stabilization capacity. They also indicate that the stability of MHC/peptide complexes can and should not be exclusively used for the prediction of immunogenicity. Our results also suggest that higher attention should be given to the possibilities to rigidify peptides through, for example, proline substitutions to enhance T cell recognition complexes.

The interdependency of different peptide residues, such as p3L and p5M in wild-type Trh4, is evident from simultaneous structural and mutations analyses. We have previously demonstrated that mutation of either p3L or p5M to an alanine abolished recognitionbyLnB5(12). InH-2D$^b$/Trh4, the bulkier side chain of p3L and the intrinsic properties of the side chain of p5M, which carries a sulfur atom, results in an unconventional peptide binding mainly through the formation of multiple sulfur–p and van der Waals interactions between the side chain of p5M and the H-2D$^b$ residues W73 and Y156 (Supplemental Fig. 2B). In H-2D$^b$/Trh4-p3P, this complex network of interactions between p5M and the H-2D$^b$ residues is abolished (Supplemental Fig. 2D), explaining the reduced overall stability of H-2D$^b$/Trh4p3P compared with H-2D$^b$/Trh4 (Fig. 2B, 2C). Instead, the conformation of the side chain of p5M is profoundly affected, with a shift of 1.4 A for the sulfur atom and 4.2 Afor the terminal methyl group, altogether resulting in large movement toward p3P and the polar H-2D$^b$ residue Gln$^{97}$, which is energetically unfavorable (Fig. 4, Supplemental Fig. 2C, 2D). Still, these modifications do not affect the overall surface of H-2D$^b$/ Trh4-p3P compared with H-2D$^b$/Trh4, keeping molecular mimicry between these two complexes (Fig. 4). Thus, the possible rigidification of the modified complex facilitates recognition by the H-2D$^b$/Trh4-specific TCR LnB5, and the similarities between the two complexes allow for effective cross-reactivity (Supplemental Fig. 2).

Finally, and in our opinion, the most important result presented within the present study is that vaccination with Trh4-p3P results in significantly higher immunogenicity, inducing much stronger CD8$^+$ T cell responses toward Trh4-presenting target cells compared with vaccination with the wild-type epitope Trh4 (Fig. 1). Collectively, our results demonstrate that TEIPP-specific CD8$^+$ T cells, promising candidates in the treatment of tumors that have escaped from conventional immunotherapies, can be successfully elicited to significantly enhance recognition of cancer target cells.

## Acknowledgments

Diffraction data were collected on beam line MX 14.1 at the BESSY II electron storage ring operated by the Helmholtz-Zentrum Berlin, Germany. We thank the crystallization facility in the Protein Science Facility at the Karolinska Institutet.

## Disclosures

The authors have no financial conflicts of interest.

## References


1. Carretero, R., J. M. Romero, F. Ruiz-Cabello, I. Maleno, F. Rodriguez, F. M. Camacho, L. M. Real, F. Garrido, and T. Cabrera. 2008. Analysis of HLA class I expression in progressing and regressing metastatic melanoma lesions after immunotherapy. Immunogenetics 60: 439–447.
2. Zaretsky, J. M., A. Garcia-Diaz, D. S. Shin, H. Escuin-Ordinas, W. Hugo, S. Hu-Lieskovan, D. Y. Torrejon, G. Abril-Rodriguez, S. Sandoval, L. Barthly, et al. 2016. Mutations associated with acquired resistance to PD-1 blockade in melanoma. N. Engl. J. Med. 375: 819–829.
3. Gao, J., L. Z. Shi, H. Zhao, J. Chen, L. Xiong, Q. He, T. Chen, J. Roszik, C. Bernatchez, S. E. Woodman, et al. 2016. Loss of IFN-g pathway genes in tumor cells as a mechanism of resistance to anti-CTLA-4 therapy. Cell 167: 397– 404.e9.
4. Chambers, B., P. Grufman, V. Fredriksson, K. Andersson, M. Roseboom, S. Laban, M. Camps, E. Z. Wolpert, E. J. H. J. Wiertz, R. Offringa, et al. 2007. Induction of protective CTL immunity against peptide transporter TAP-deficient tumors through dendritic cell vaccination. Cancer Res. 67: 8450–8455.
5. Doorduijn, E. M., M. Sluijter, B. J. Querido, C. C. Oliveira, A. Achour, F. Ossendorp, S. H. van der Burg, and T. van Hall. 2016. TAP-independent self-peptides enhance T cell recognition of immune-escaped tumors. J. Clin. Invest. 126: 784–794.
6. Oliveira, C. C., B. Querido, M. Sluijter, A. F. de Groot, R. van der Zee, M. J. W. E. Rabelink, R. C. Hoeben, F. Ossendorp, S. H. van der Burg, and T. van Hall. 2013. New role of signal peptide peptidase to liberate C-terminal peptides for MHC class I presentation. J. Immunol. 191: 4020–4028.
7. Oliveira, C. C., M. Sluijter, B. Querido, F. Ossendorp, S. H. van der Burg, and T. van Hall. 2014. Dominant contribution of the proteasome and metal-loproteinases to TAP-independent MHC-I peptide repertoire. Mol. Immunol. 62: 129–136.
8. Oliveira, C. C., P. A. van Veelen, B. Querido, A. de Ru, M. Sluijter, S. Laban, J. W. Drijfhout, S. H. van der Burg, R. Offringa, and T. van Hall. 2010. The nonpolymorphic MHC Qa-1b mediates CD8$^+$ T cell surveillance of antigen-processing defects. [Published erratum appears in 2010 J. Exp. Med. 207: 671.] J. Exp. Med. 207: 207–221.
9. Oliveira, C. C., and T. van Hall. 2015. Alternative antigen processing for MHC class I: multiple roads lead to Rome. Front. Immunol. 6: 298.
10. van Hall, T., E. Z. Wolpert, P. van Veelen, S. Laban, M. van der Veer, M. Roseboom, S. Bres, P. Grufman, A. de Ru, H. Meiring, et al. 2006. Selective cytotoxic T-lymphocyte targeting of tumor immune escape variants. Nat. Med. 12: 417–424.
11. Doorduijn, E. M., M. Sluijter, K. A. Marijt, B. J. Querido, S. H. van der Burg, and T. van Hall. 2017. T cells specific for a TAP-independent self-peptide remain naive in tumor-bearing mice and are fully exploitable for therapy. OncoImmunology 7: e1382793.
12. Hafstrand, I., E. M. Doorduijn, A. D. Duru, J. Buratto, C. C. Oliveira, T. Sandalova, T. van Hall, and A. Achour. 2016. The MHC class I cancer-associated neoepitope Trh4 linked with impaired peptide processing induces a unique noncanonical TCR conformer. J. Immunol. 196: 2327–2334.
13. Riebeling, C., J. C. Allegood, E. Wang, A. H. Merrill, Jr., and A. H. Futerman. 2003. Two mammalian longevity assurance gene (LAG1) family members, trh1 and trh4, regulate dihydroceramide synthesis using different fatty acyl-CoA donors. J. Biol. Chem. 278: 43452–43459.
14. Wang, Z., R. Turner, B. M. Baker, and W. E. Biddison. 2002. MHC allelespecific molecular features determine peptide/HLA-A2 conformations that are recognized by HLA-A2-restricted T cell receptors. J. Immunol. 169: 3146–3154.
15. van Stipdonk, M. J. B., D. Badia-Martinez, M. Sluijter, R. Offringa, T. van Hall, and A. Achour. 2009. Design of agonistic altered peptides for the robust induction of CTL directed towards H-2D$^b$ in complex with the melanomaassociated epitope gp100. Cancer Res. 69: 7784–7792.
16. Qiu, Z., H. Huang, J. M. Grenier, O. A. Perez, H. M. Smilowitz, B. Adler, and K. M. Khanna. 2015. Cytomegalovirus-based vaccine expressing a modified tumor antigen induces potent tumor-specific CD8$^+$ T-cell response and protects mice from melanoma. Cancer Immunol. Res. 3: 536–546.
17. Qiu, Z., J. M. Grenier, and K. M. Khanna. 2015. Reviving virus based cancer vaccines by using cytomegalovirus vectors expressing modified tumor antigens. OncoImmunology 5: e1056974.
18. Uchtenhagen, H., E. T. Abualrous, E. Stahl, E. B. Allerbring, M. Sluijter, M. Zacharias, T. Sandalova, T. van Hall, S. Springer, P.-Å. Nygren, A. and A. Achour. 2013. Proline substitution independently enhances H-2D$^b$ complex stabilization and TCR recognition of melanoma-associated peptides. Eur. J. Immunol. 43: 3051–3060.
19. Rasmussen, M.,E. Fenoy,M.Harndahl,A. B. Kristensen,I. K.Nielsen,M.Nielsen, and S. Buus. 2016. Pan-specific prediction of peptide-MHC class I complex stability, a correlate of T cell immunogenicity. J. Immunol. 197: 1517–1524.
20. Achour, A., R. A. Harris, K. Persson, J. Sundba¨ck, C. L. Sentman, G. Schneider, Y. Lindqvist, and K. Ka¨rre. 1999. Murine class I major histocompatibility complex H-2D$^d$: expression, refolding and crystallization. Acta Crystallogr. D Biol. Crystallogr. 55: 260–262.
21. Achour, A., K. Persson, R. A. Harris, J. Sundba¨ck, C. L. Sentman, Y. Lindqvist, G. Schneider, and K. Ka¨rre. 1998. The crystal structure of H-2D$^b$ MHC class I complexed with the HIV-1-derived peptide RAHYNIVTF reveals modifications for T cell and NK cell recognition. Immunity 9: 199–208.
22. Achour, A., J. Michae¨lsson, R. A. Harris, J. Odeberg, P. Grufman, J. K. Sandberg, V. Levitsky, K. Ka¨rre, T. Sandalova, and G. Schneider. 2002. A structural basis for LCMV immune evasion: subversion of H-2D$^b$ and H-2K$^b$ presentation of gp33 revealed by comparative crystal structure.Analyses. Immunity 17: 757–768.
23. Allerbring, E. B., A. D. Duru, H. Uchtenhagen, C. Madhurantakam, M. B. Tomek, S. Grimm, P. A. Mazumdar, R. Friemann, M. Uhlin, T. Sandalova, et al. 2012. Unexpected T-cell recognition of an altered peptide ligand is driven by reversed thermodynamics. Eur. J. Immunol. 42: 2990–3000.
24. Pellegrino, S., C. Annoni, A. Contini, F. Clerici, and M. L. Gelmi. 2012. Expedient chemical synthesis of 75mer DNA binding domain of MafA: an insight on its binding to insulin enhancer. Amino Acids 43: 1995–2003.
25. Sandalova, T., J. Michae¨lsson, R. A. Harris, J. Odeberg, G. Schneider, K. Ka¨rre, and A. Achour. 2005. A structural basis for CD8$^+$ T cell-dependent recognition of non-homologous peptide ligands: implications for molecular mimicry in autoreactivity. J. Biol. Chem. 280: 27069–27075.
26. Sandalova, T., J. Michae¨lsson, R. A. Harris, H.-G. Ljunggren, K. Ka¨rre, G. Schneider, and A. Achour. 2005. Expression, refolding and crystallization of murine MHC class I H-2D$^b$ in complex with human b$_2$-microglobulin. Acta Crystallogr. Sect. F Struct. Biol. Cryst. Commun. 61: 1090–1093.
27. Leslie, A. G. W. 2006. The integration of macromolecular diffraction data. Acta Crystallogr. D Biol. Crystallogr. 62: 48–57.
28. Evans, P. R., and G. N. Murshudov. 2013. How good are my data and what is the resolution? Acta Crystallogr. D Biol. Crystallogr. 69: 1204–1214.
29. McCoy, A. J., R. W. Grosse-Kunstleve, P. D. Adams, M. D. Winn, L. C. Storoni, and R. J. Read. 2007. Phaser crystallographic software. J. Appl. Cryst. 40: 658–674.
30. Velloso, L. M., J. Michae¨lsson, H.-G. Ljunggren, G. Schneider, and A. Achour. 2004. Determination of structural principles underlying three different modes of lymphocytic choriomeningitis virus escape from CTL recognition. J. Immunol. 172: 5504–5511.
31. Winn, M. D., G. N. Murshudov, and M. Z. Papiz. 2003. Macromolecular TLS refinement in REFMAC at moderate resolutions. Methods Enzymol. 374: 300–321.
32. Adams, P. D., P. V. Afonine, G. Bunko´czi, V. B. Chen, I. W. Davis, N. Echols, J. J. Headd, L. W. Hung, G. J. Kapral, R. W. Grosse-Kunstleve, et al. 2010. PHENIX: a comprehensive Python-based system for macromolecular structure solution. Acta Crystallogr. D Biol. Crystallogr. 66: 213–221.
33. Emsley, P., and K. Cowtan. 2004. Coot: model-building tools for molecular graphics. Acta Crystallogr. D Biol. Crystallogr. 60: 2126–2132.
34. Deres, K., W. Beck, S. Faath, G. Jung, and H.-G. Rammensee. 1993. MHC/ peptide binding studies indicate hierarchy of anchor residues. Cell. Immunol. 151: 158–167.
35. Zhou, X., U. M. Abdel Motal, L. Berg, and M. Jondal. 1992. In vivo priming of cytotoxic T lymphocyte responses in relation to in vitro up-regulation of major histocompatibility complex class I molecules by short synthetic peptides. Eur. J. Immunol. 22: 3085–3090.
36. Achour, A., J. Michae¨lsson, R. A. Harris, H. G. Ljunggren, K. Ka¨rre, G. Schneider, and T. Sandalova. 2006. Structural basis of the differential stability and receptor specificity of H-2D$^b$ in complex with murine versus human b$_2$microglobulin. J. Mol. Biol. 356: 382–396.
37. Hicklin, D. J., F. M. Marincola, and S. Ferrone. 1999. HLA class I antigen downregulation in human cancers: T-cell immunotherapy revives an old story. Mol. Med. Today 5: 178–186.
38. Leone, P., E.-C. Shin, F. Perosa, A. Vacca, F. Dammacco, and V. Racanelli. 2013. MHC class I antigen processing and presenting machinery: organization, function, and defects in tumor cells. J. Natl. Cancer Inst. 105: 1172–1187.
39. Campoli, M., and S. Ferrone. 2008. HLA antigen changes in malignant cells: epigenetic mechanisms and biologic significance. Oncogene 27: 5869–5885.
40. Chen, J.-L., G. Stewart-Jones, G. Bossi, N. M. Lissin, L. Wooldridge, E. M. L. Choi, G. Held, P. R. Dunbar, R. M. Esnouf, M. Sami, et al. 2005. Structural and kinetic basis for heightened immunogenicity of T cell vaccines. J. Exp. Med. 201: 1243–1255.
41. Webb, A. I., M. A. Dunstone, W. Chen, M.-I. Aguilar, Q. Chen, H. Jackson, L. Chang, L. Kjer-Nielsen, T. Beddoe, J. McCluskey, et al. 2004. Functional and structural characteristics of NY-ESO-1-related HLA A2-restricted epitopes and the design of a novel immunogenic analogue. J. Biol. Chem. 279: 23438–23446.
42. van der Burg, S. H., M. J. W. Visseren, R. M. Brandt, W. M. Kast, and C. J. M. Melief. 1996. Immunogenicity of peptides bound to MHC class I molecules depends on the MHC-peptide complex stability. J. Immunol. 156: 3308–3314.
43. Harndahl, M., M. Rasmussen, G. Roder, I. Dalgaard Pedersen, M. Sørensen, M. Nielsen, and S. Buus. 2012. Peptide-MHC class I stability is a better predictor than peptide affinity of CTL immunogenicity. Eur. J. Immunol. 42: 1405–1416.
44. Ilyushkin, O. Y., F. K. Insaidoo, T. K. Baxter, D. J. Powell, Jr., L. A. Johnson, N. P. Restifo, and B. M. Baker. 2007. Structures of MART-126/27-35 peptide/HLA-A2 complexes reveal a remarkable disconnect between antigen structural homology and T cell recognition. J. Mol. Biol. 372: 1123–1136.
45. Borbulevych, O. Y., K. H. Piepenbrink, B. E. Gloor, D. R. Scott, R. F. Sommese, D. K. Cole, A. K. Sewell, and B. M. Baker. 2009. T cell receptor cross-reactivity directed by antigen-dependent tuning of peptide-MHC molecular flexibility. Immunity 31: 885–896.
46. Insaidoo, F. K., O. Y. Borbulevych, M. Hossain, S. M. Santhanagopolan, T. K. Baxter, and B. M. Baker. 2011. Loss of T cell antigen recognition arising from changes in peptide and major histocompatibility complex protein flexibility: implications for vaccine design. J. Biol. Chem. 286: 40163–40173.
47. Duan, F., J. Duitama, S. Al Seesi, C. M. Ayres, S. A. Corcelli, A. P. Pawashe, T. Blanchard, D. McMahon, J. Sidney, A. Sette, et al. 2014. Genomic and

bioinformatic profiling of mutational neoepitopes reveals new rules to predict anticancer immunogenicity. J. Exp. Med. 211: 2231–2248.

48. Suzuki, Y., K. Oishi, H. Nakano, and T. Nagayama. 1987. A strong correlation between the increase in number of proline residues and the rise in thermostability of five Bacillus oligo-1,6-glucosidases. Appl. Microbiol. Biotechnol. 26: 546–551.

49. Watanabe, K., T. Masuda, H. Ohashi, H. Mihara, and Y. Suzuki. 1994. Multiple proline substitutions cumulatively thermostabilize Bacillus cereus ATCC7064 oligo-1,6-glucosidase. Irrefragable proof supporting the proline rule. Eur. J. Biochem. 226: 277–283.

50. Haidar, J. N., W. Zhu, J. Lypowy, B. G. Pierce, A. Bari, K. Persaud, X. Luna, M. Snavely, D. Ludwig, and Z. Weng. 2014. Backbone flexibility of CDR3 and immune recognition of antigens. J. Mol. Biol. 426: 1583–1599.

51. Jimenez, R., G. Salazar, K. K. Baldridge, and F. E. Romesberg. 2003. Flexibility and molecular recognition in the immune system. Proc. Natl. Acad. Sci. USA 100: 92–97.

52. Vanhoof, G., F. Goossens, I. De Meester, D. Hendriks, and S. Scharpe´. 1995. Proline motifs in peptides and their biological processing. FASEB J. 9: 736–744.

# Supplementary Figure 1

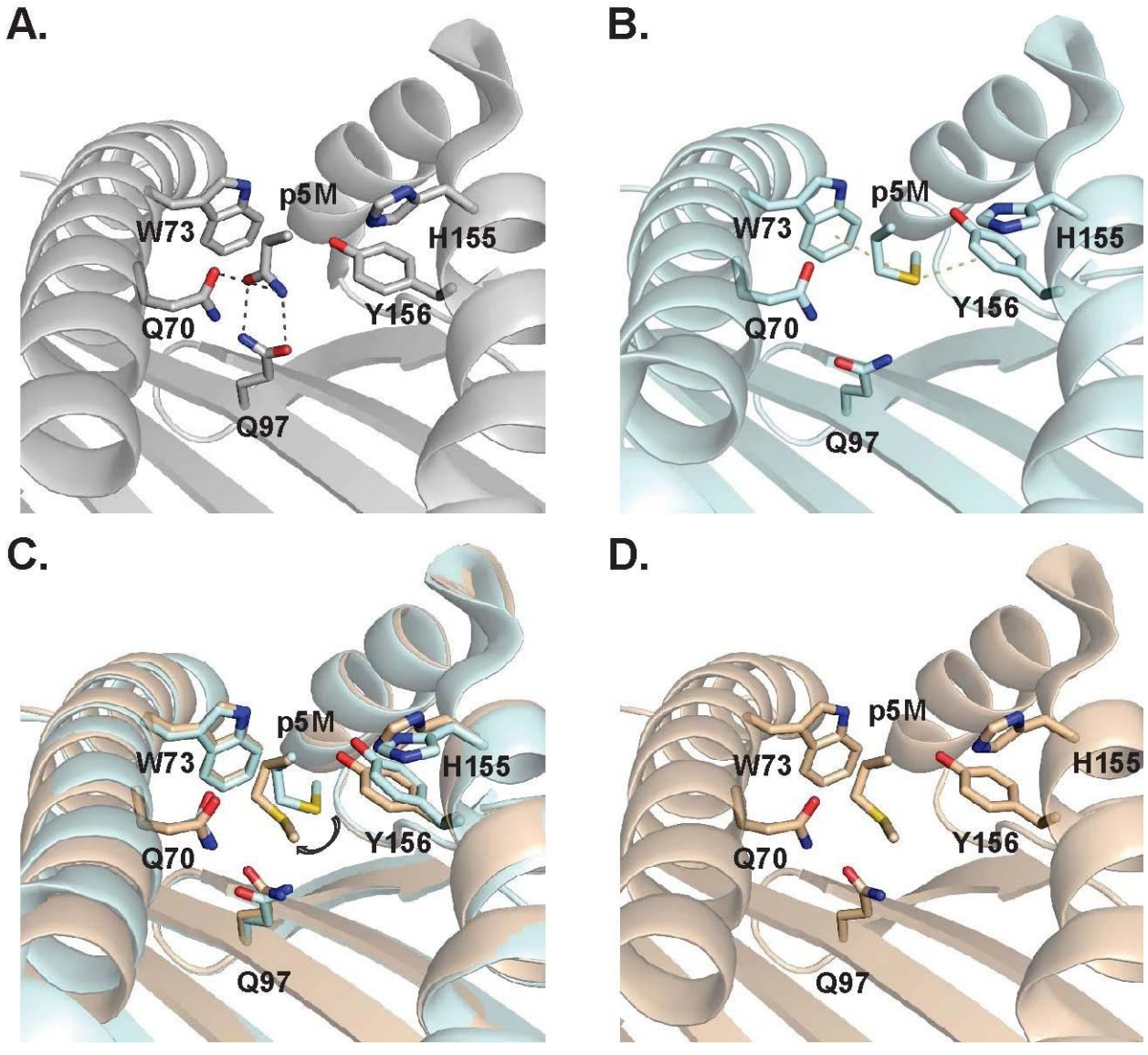


**Supplementary Figure 1. The conformational shift of p5M in H-2D$^b$/Trh4-p3P abrogates sulfur-**S **interactions,explainingthe reducedstabilityoftheMHC/peptidecomplex A)** The prototypic main anchor residue asparagine at position 5 of the H-2D$^b$-restricted epitope gp33 (1S7U) formshydrogenbonds(greydashes)withthesidechainoftheH-2D$^b$ heavychainresiduesQ70andQ97. **B)** The sulfur atomin the main anchor residue p5M in wild-type Trh4 (5E8N) formssulfur-S_yellow dashes_and vanderWaalsinteractionswiththeH-2D$^b$ residuesW73andY156. **C)** Thep3Psubstitution(residue notshown)causes a shiftintheconformationofthesidechainofp5Maswell as theH-2D$^b$ residuesY156andH155. **D)** The conformational shift of peptide residue p5M in Thr4-p3P abolishes the sulfur-S interactions formed between the sulfur tip of p5M and both Y156 and W73 present in H-2D$^b$/Trh4, and previously demonstrated as essential for the stability of the MHC/peptide complex. Only the side chain of peptide residue p5 is shown for clarity.

# Supplementary Figure 2

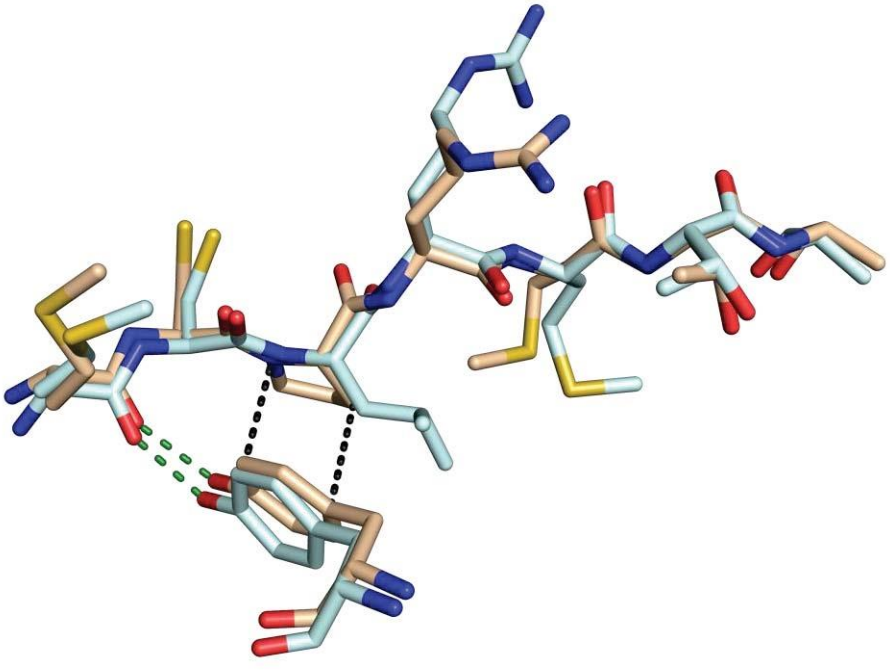

**Supplementary Figure 2. The side chain of p3P forms CH-π and van der Waals interactions with the heavy chain residue Y159**

The side chain of the proline residue p3P forms CH-S and van der Waals interactions with the heavy chain residue Y159 (black dashed lines). The hydrogen bond formed between Y159 and the main chain oxygen of p1M is displayed as a green dashed line. H-2D$^{b}$/Trh4 and H-2D$^{b}$/Trh4-p3P residues are displayed in light blue and wheat, respectively. Negatively and positively charged atoms are in red and blue, respectively.

# Supplementary Table I

| | H-2D$_b$/Trh4-p3P |
|---|---|
| PDB code | **5MZM** |
| **Data collection** | |
| Spacegroup | I 1 2 1 |
| Cell dimensions a, b, c (Å) | 91.35, 125.01, 98.05 |
| α, β, γ (°) | 90.0, 103.53, 90.0 |
| Resolution (Å) | 58.5-2.4 (2.49-2.40) |
| No of reflections | 41766 (4378) |
| $R_{merge}$ [1] | 0.087 (0.29) |
| I/σ(I) | 7.0 (2.1) |
| Multiplicity | 3.6 (3.6) |
| Completeness (%) | 99.9 (100.0) |
| CC (1/2) | 0.991 (0.913) |
| | |
| **Refinement statistics** | |
| $R_{cryst}$/$R_{free}$ (%) | 22.63/26.81 |
| Mean B-factor (Å$^2$) | 48.96 |
| | |
| Deviations from ideal values | |
| Bond length (Å) | 0.003 |
| Bond angles (°) | 0.657 |
| | |
| Ramachandran plot | |
| In favoured region (%) | 97.02 |
| Outliers (%) | 0.14 |

Values in parentheses are for the highest resolution shell.

[1] $R_{merge} = \sum_{hkl} \sum_i | I_i(hkl) - \langle I(hkl) \rangle | / \sum_{hkl} \sum_i I_i(hkl)$, where $I_i(hkl)$ is the $i$th observation of reflection $hkl$ and $\langle I(hkl) \rangle$ is the weighted average intensity for all observations $i$ of reflection hkl.

[2] $R_{cryst} = \Sigma||F_o| - |F_c||/\Sigma|F_o|$, where $|F_o|$ and $|F_c|$ are the observed and calculated structure factor amplitudes of a particular reflection and the summation is over 95 % of the reflections in the specified resolution range. The remaining 5 % of the reflections were randomly selected (test set) before the structure refinement and not included in the structure refinement.

[3] $R_{free}$ was calculated over these reflections using the same equation as for $R_{cryst}$.

**Supplementary Table I. Data collection and refinement statistics**